Original Research
Basic Implantodontology and Biomaterials

Histomorphometric evaluation of strontium-containing nanostructured hydroxyapatite as bone substitute in sheep

Callinca Paolla Gomes MACHADO[a]
Suelen Cristina SARTORETTO[a]
Adriana Terezinha Neves Novellino ALVES[a]
Inayá Barbosa Correa LIMA[b]
Alexandre Malta ROSSI[b]
José Mauro GRANJEIRO[c]
Mônica Diuana CALASANS-MAIA[d]

[a]Universidade Federal Fluminense – UFF, School of Dentistry, Graduate Program, Niterói, RJ, Brazil.

[b]Universidade Federal do Rio de Janeiro – UFRJ, Instituto Alberto Luiz Coimbra de Pós-Graduação e Pesquisa de Engenharia – Coppe, Programa de Engenharia Nuclear, Rio de Janeiro, RJ, Brazil.

[c]Universidade Federal Fluminense – UFF, School of Dentistry, Niteroi, RJ, Brazil. OU Instituto Nacional de Metrologia, Qualidade e Tecnologia – Inmetro, Duque de Caxias, RJ, Brazil.

[d]Universidade Federal Fluminense – UFF, School of Dentistry, Department of Oral Surgery, Niterói, RJ, Brazil.

Declaration of Interests: The authors certify that they have no commercial or associative interest that represents a conflict of interest in connection with the manuscript.

Corresponding Author:
Mônica Diuana Calasans-Maia
E-mail: monicacalasansmaia@gmail.com

DOI: 10.1590/1807-3107BOR-2016.vol30.0045

Submitted: Jul 08, 2015
Accepted for publication: Nov 11, 2015
Last revision: Jan 25, 2016

Abstract: The aim of this study is to evaluate the biocompatibility and osteoconductivity in surgical defects of sheep tibias filled with 1% strontium-containing nanostructured hydroxyapatite microspheres (SrHA), stoichiometric hydroxyapatite without strontium microspheres (HA), or blood clots. Santa Ines sheep were subjected to three perforations on the medial side of the left tibia. The biomaterials were characterized by X-ray Diffraction (XRD) and Fourier Transform Infrared (FTIR) before implantation and by X-Ray Microfluorescence (μFRX) and Scanning Electron Microscopy (SEM) after sheep tibias implantation. Surgical defects were filled with blood clots (control), SrHA (Group 1) or HA (Group 2). After 30 days, 5-μm bone blocks were obtained for histological evaluation, and the blocks obtained from 1 animal were embedded in methylmethacrylate for undecalcified sections. Mononuclear inflammatory infiltrate remained mild in all experimental groups. Giant cells were observed surrounding biomaterials particles of both groups and areas of bone formation were detected in close contact with biomaterials. All groups showed newly formed bone from the periphery to the center of the defects, which the control, HA and SrHA presented 36.4% (± 21.8), 31.2% (± 14.7) and 26.2% (± 12.9) of newly formed bone density, respectively, not presenting statistical differences. In addition, the connective tissue density did not show any significant between groups. The SrHA showing a higher volume density of biomaterial (51.2 ± 14.1) present in the defect compared to HA (32.6 ± 8.5) after 30 days ($p = 0.03$). Microspheres containing 1% SrHA or HA can be considered biocompatible, have osteoconductive properties and may be useful biomaterials for clinical applications.

Keywords: Bone Regeneration; Histology; Models, Animal.

Introduction

Bone and joint degenerative and inflammatory problems affect millions of people worldwide. In fact, they account for half of all chronic diseases in people over 50 years of age in developed countries. Various methods have been applied for the restoration of bone defects and preservation of bone morphology,[1,2] and several techniques for bone restoration have been developed and improved in recent years, including bone block grafts, guided bone regeneration, distraction osteogenesis, and the use of new biomaterials and growth factors.[3,4,5] Although autogenous bone

graft is considered the gold standard,[6,7] its use may be limited due to the morbidity related to the need for other donor sites.[8] Consequently, the development of alternative materials has increased. Calcium phosphates, especially the compounds hydroxyapatite (HA) and tricalcium phosphate (TCP), have been investigated as materials for bone regeneration for 80 years. Synthetic HA is usually employed in the form of coarse particles, with crystal morphology that is quite different from the biological apatite in bone.[9]

Among the many cations that can substitute for calcium in the structure of hydroxyapatite (HA), strontium is attracting increasing interest because of its beneficial effects on bone formation and prevention of bone resorption.[10] A recent study has shown that the osteoconductivity of 20% strontium-containing hydroxyapatite (SrHA) used as a coating on implant surfaces results not only in an acceleration but also an improvement in bone-implant integration.[11] There is evidence that strontium (Sr^{2+}) has a beneficial effect on bone[12,13,14] by increasing osteoblast activity and decreasing osteoclast activity.[15,16,17] Previous studies[18,19,20] have demonstrated an increase in the thickness of the bone layer formed on the bone-cement interface and better osseointegration of strontium-containing HA cement, but additional *in vivo* studies are desirable. The purpose of this investigation was to evaluate bone healing after implantation of microspheres of HA and 1% strontium-containing nanostructured hydroxyapatite (SrHA) in sheep tibias.

Methodology

Synthesis of biomaterials

Hydroxyapatite powder (<74 µm) containing 1% (w/w) strontium (SrHA) and stoichiometric hydroxyapatite (control group) were mixed with a solution of sodium alginate (1% w/v) with mild agitation to form a ceramic slurry. For extrusion, the ceramic slurry was then dripped into a solution of calcium chloride ($CaCl_2$, 0.15 M), in which spheres formed immediately. The spheres were left in the calcium chloride solution for 24 hours and were then washed 5 times with 500 mL ultrapure water (MilliQ®, Millipore Corp.) and lyophilized. After 24 hours, they were placed into alumina trays and sintered to 1100 °C in a muffle furnace for 27 hours. The spheres obtained were sifted using sieves with openings ranging from 425 to 600 µm in size, sterilized in a stove at 200 °C for 2 hours and sealed prior to performing the surgical procedure. The syntheses of the biomaterials were performed at the *Laboratório de Biomateriais* – LABIOMAT at the *Centro Brasileiro de Pesquisas Físicas* – CBPF, Rio de Janeiro, Brazil.

Characterization of the powders

The crystalline mineral phases present in the samples and their crystallinities were examined by X-ray diffraction (XRD). The XRD patterns were obtained with a HZG4 diffractometer operating at 30 kV and 15mA with CuKα radiation (λ = 1.542 Å). The data were collected in the 2θ range of 10°–100° with a step of 0.02° point per second. The vibrational modes of the phosphate and hydroxyl groups in the SrHA samples were analyzed by Fourier transform infrared spectroscopy. The spectra were obtained with an FTIR-IR—Prestige 21 (Shimadzu) operating in transmission mode from 400 to 4000 cm^{-1}.

Animals

Six mature Santa Ines female sheep, weighing between 31 and 35 kg, were obtained from the Veterinary Medicine School of *Universidade Federal Fluminense* – UFF, and the surgical procedures were performed at the Laboratory of Animal Experimentation of the Veterinary School of UFF. The conditions for the animal experiments and breeding were approved by the Institutional Review Board (*Comissão de Ética no Uso de Animais* – CEUA/UFF) no. 184, in compliance with the NIH Guide for the Care and Use of Laboratory Animals and with Brazilian legislation on animal experimentation.

Surgical procedures

All animals were pre-anesthetized with acepromazin 0.1 $mg.kg^{-}$ (Acepran®, Vetnil, Louveira, Brazil), diazepam 0.2 $mg.kg^{-1}$ (Diazepam®, União Química, Embu-Guaçu, Brazil) and morphine 0.4 $mg.kg^{-1}$ (Dimorf®, Cristália, São Paulo, Brazil). Then, they were anesthetized with propofol 4 $mg.kg^{-1}$ (Propofol®, Biosintética, São Paulo, Brazil) and diazepam 0.1 $mg.kg^{-1}$ (Diazepam®, União Química,

Embu-Guaçu, Brazil) and maintained under anesthesia with 1% of isoflurane (Isoflurane, Cristália, São Paulo, Brazil). Following administration of anesthesia and trichotomy, a 4-cm incision was made in the epithelial lining of the animal's leg. After exposure of the tibia bone surface and under constant saline irrigation, three holes separated by a 1-cm margin were created by drilling; each hole measured 2 mm in diameter and penetrated the cortices of the left tibia in a direction perpendicular to the bone axis. The bone defects were filled with microspheres of HA, clots and microspheres of SrHA, respectively, in the craniocaudal direction (Figure 1A). The tissue flap was then returned to its original position, and the incision was closed with interrupted #5-0 nylon sutures (Mononylon Ethicon, Johnson & Johnson, São Paulo, Brazil). After surgery, the sheep were allowed to move and eat, and the wound was left uncovered. As a postoperative protocol to prevent infection and control pain, all animals were injected intramuscularly with 0.5 $mg.kg^{-1}$ meloxicam (Maxicam®, Ourofino, Cravinhos, Brazil) for five days and 5 $mg.kg^{-1}$ enrofloxacin (Enrofloxacin®, Tortuga, São Paulo, Brazil) before surgery and for five days following all surgical procedures.

After the 30-day experimental period, the animals were anesthetized, and an incision was created at the site of implant installation to remove the samples with a trephine bur (Ø = 6 mm) (Figure 1B and 1C). The animals were kept alive after the second surgery, and the protocols for suturing and postoperative care were the same as those for the first surgery. Three fragments, each containing microspheres and bone from the tibia, were collected from five animals (Figure 1D). All animals in this study remained confined for a period of 30 days after biopsy removal.

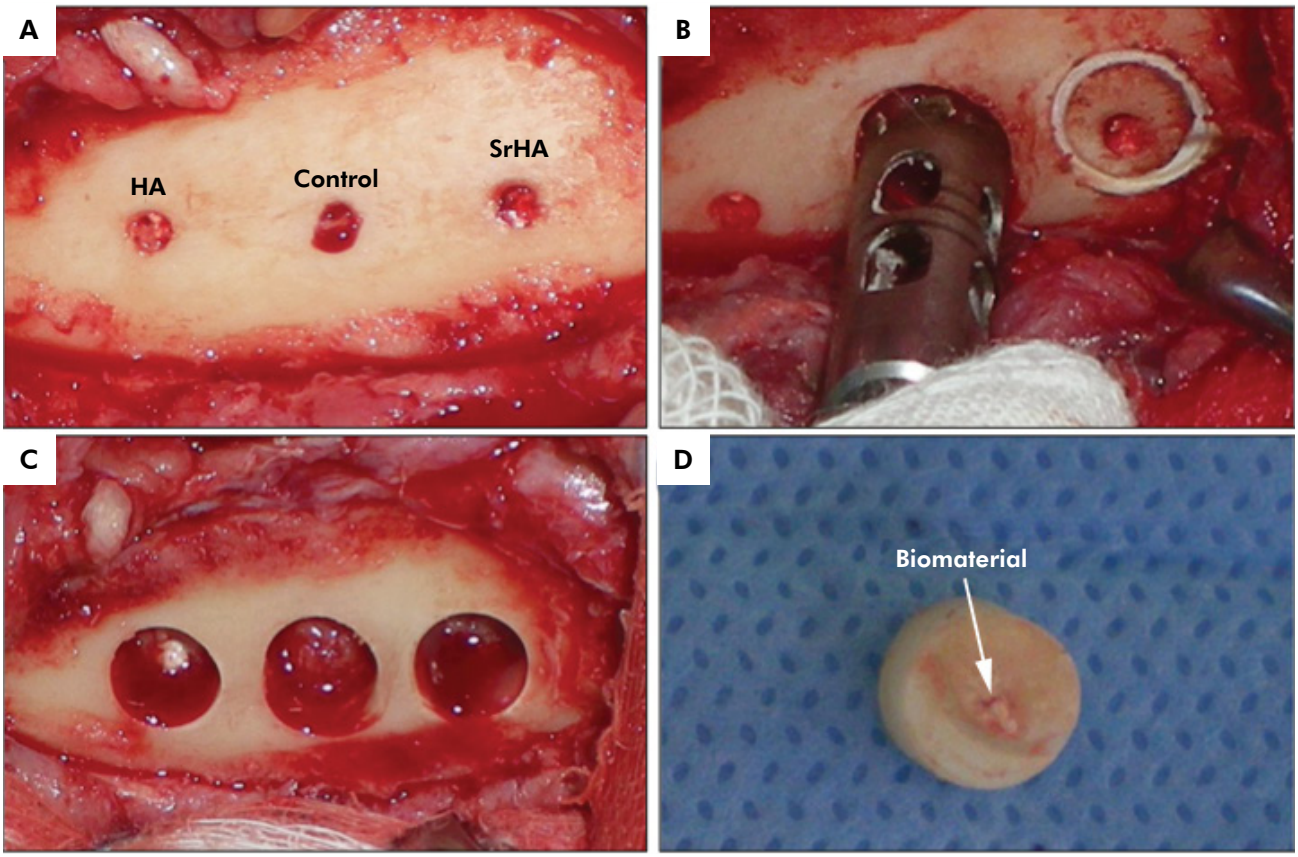

Figure 1. (A) Sheep tibia region of biomaterial placement; (B) trephine bur (Ø 6 mm) used to collect samples from the tibia; (C) sheep tibia after bone block removal for histological evaluation; (D) bone block containing biomaterial microspheres obtained after 30 days of implantation. This technique allows for the maintenance of live animals after the experiment.

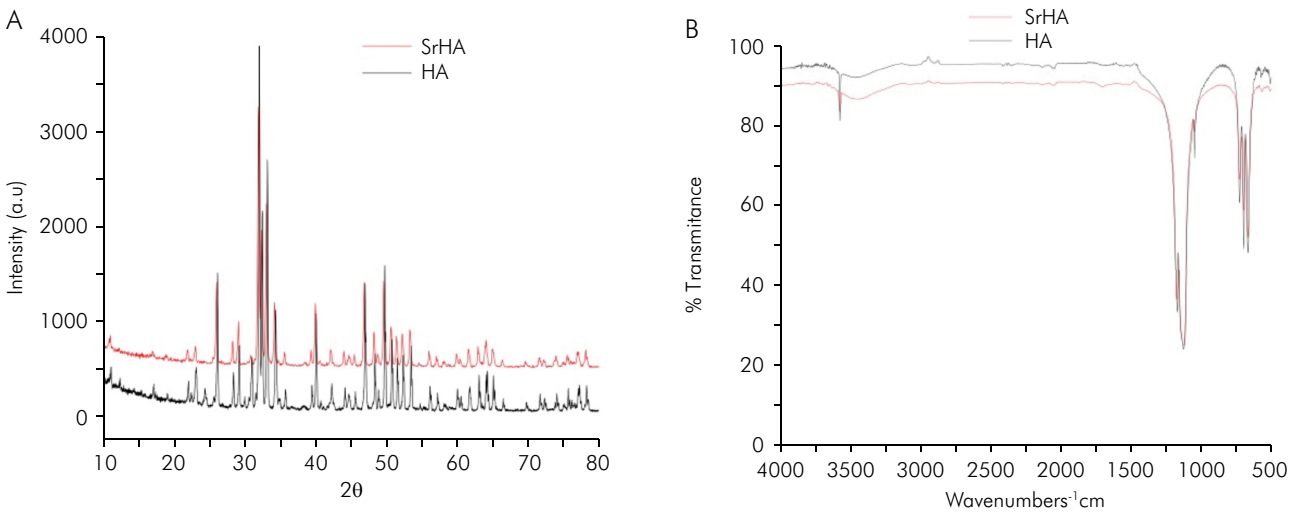

Figure 2. (A) X-ray diffraction (XRD) of SrHA (red) and HA (black) samples. (B) Fourier transform infrared (FTIR) spectra of SrHA (red) and HA (black) samples.

Histological analysis

A single histologist who was blinded to the group assignments of the samples performed histological analysis. The specimens were fixed in 4% buffered formalin for 48 hours and demineralized for 24 hours (Allkimia®, EDTA solution) prior to histological processing for paraffin embedding. Paraffin serial sections of 5 µm thickness were obtained and stained with hematoxylin–eosin (HE) for histological analysis and histomorphometric evaluation. To prepare undecalcified bone sections, three fragments were collected from one animal and fixed in 70% ethanol, dehydrated in successive ethanol solutions and then impregnated and embedded in methyl methacrylate. Two histological sections were obtained from each undecalcified block that were cut at thicknesses of 30-50 µm and 100 µm, respectively, to acquire coronal sections of the tibia. The unstained, polished 30-50 µm sections were analyzed by energy dispersive spectrometry with a scanning electron microscope (SEM- JEOL JSM 5310).

X-ray microfluorescence with synchrotron radiation

The 100 µm resin sections were analyzed by elemental mapping performed under X-ray microfluorescence using synchrotron radiation on a D09-XRF beam line (µXRF-SR; LNLS, Campinas, Brazil) to qualitatively identify the interaction between the strontium of the biomaterial and biological medium and the components present in the regions of interest (the defect where the biomaterials were placed and the surrounding areas). The XRF spectrometer was operated at 40 kV and 50 mA with a Ge (111) crystal, a collimator of 550 µm and a flow detector for the KV lines of calcium, strontium, potassium and zinc.[4]

Histomorphometric Evaluation

The decalcified sections were observed under a light microscope (Nikon Eclipse E400) with an objective lens at 10X magnification. Eight non-consecutive images of each specimen section were captured using a CCD camera (Evolution MP color 5.0 Media Cybernetics). The images were used for histomorphometric analysis with Image Pro-Plus 6.0® (Media Cybernetics, Inc.) to calculate the volume density of the newly formed bone and to determine the biomaterial and connective tissue densities by measuring the area of interest (AOI). The data were arranged in a table using Microsoft® Excel 2007 and analyzed statistically with GraphPad 5.0 Instat® software. The non-parametric Kruskal-Wallis test with Dunn's post-test, with a significance level of $p \leq 0.05$, were used to investigate differences in newly formed bone density and connective tissue density between the groups. The difference in biomaterial density between the groups was analyzed with the Wilcoxon signed-rank test ($p \leq 0.05$).

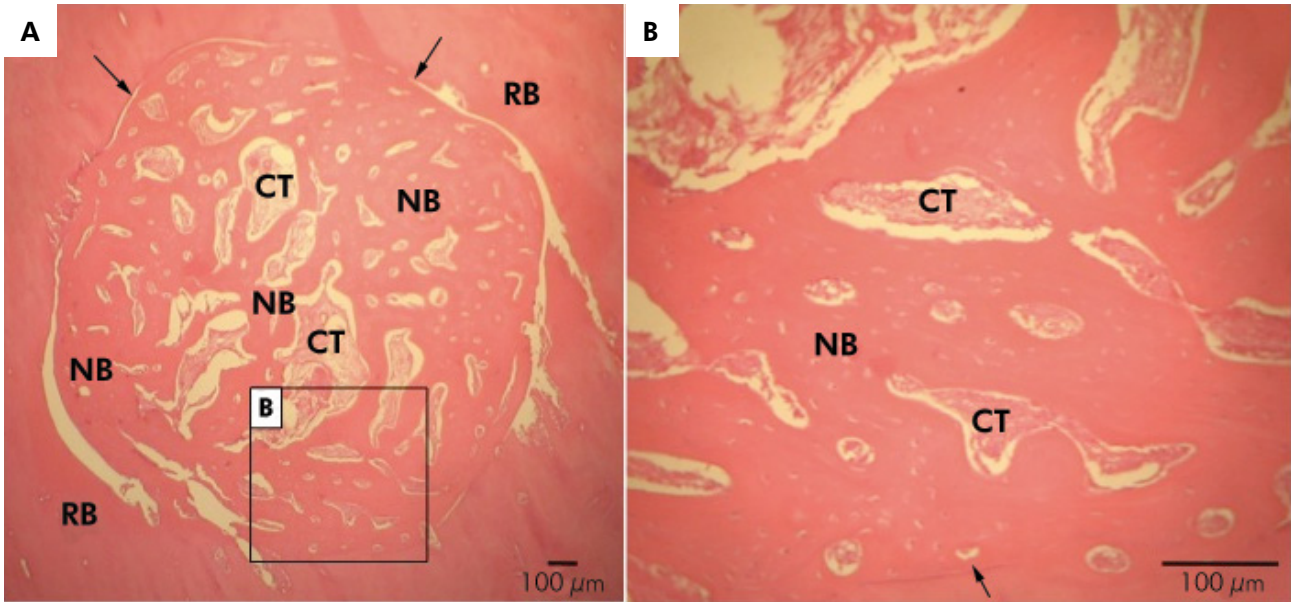

Figure 3. Representative photomicrographs of the control group. Defect area (black arrow); newly formed bone (NB) composed of wide anastomosing trabecular bone adjacent to remaining bone (RB). The central portion of the defect shows areas of connective tissue (CT). Stain: hematoxylin and eosin.

Results

Characterization of the powders

The XRD patterns for the HA and SrHA powders after sintering are depicted in Figure 2A, which shows that HA is a biomaterial with more crystallinity than SrHA. FTIR spectroscopy analysis of the SrHA and HA powders showed bands ranging from 1100 to 500 cm^{-1}, corresponding to the vibrational modes of $(PO_4)^{3-}$, and a band at 3570 cm^{-1}, corresponding to the vibrational mode of (OH^{-1}). This FTIR spectrum revealed bands typical for HA (Figure 2B).

Descriptive light microscopic evaluation

Histological evaluation revealed new bone formation from the periphery to the center of the bone defect in the control group, composed of wide anastomosing trabecular bone; however, this group also exhibited areas of connective tissue scattered around the bone defect, mainly in the central portion (Figure 3A and 3B). The HA group showed bone formation from the periphery toward the center of the defect and the presence of newly formed bone trabeculae with osteoblastic layers, but the central portion of the defect consisted of loose connective tissue with biomaterials, sparse chronic inflammatory infiltrate and few multinucleated giant cells (Figure 4A and 4B). The SrHA group exhibited bone formation from the periphery to the center, the presence of islands of loose connective tissue scattered within the defect, and sparse inflammatory infiltrate and multinucleated giant cells, predominantly lymphocytic. Large amounts of biomaterials and bone matrix were detected (Figure 5A and 5B). None of the groups showed areas of necrosis. In both implanted groups, there was intimate contact at the bone-biomaterial interface.

Scanning electron microscopy

The sample clot group presented with the expected topography for a non-critical defect after 30 days, with newly formed bone and almost all of the defect filled by trabecular bone (Figure 6A). The HA group showed no dissolution of the biomaterials, with large quantities of remnants with no signs of resorption (Figure 6B). The SrHA group also showed the presence of biomaterials in the defect without indication of resorption (Figure 6C). Energy dispersive spectroscopy was performed to evaluate the basic chemistry of the samples. The clot group had large quantities

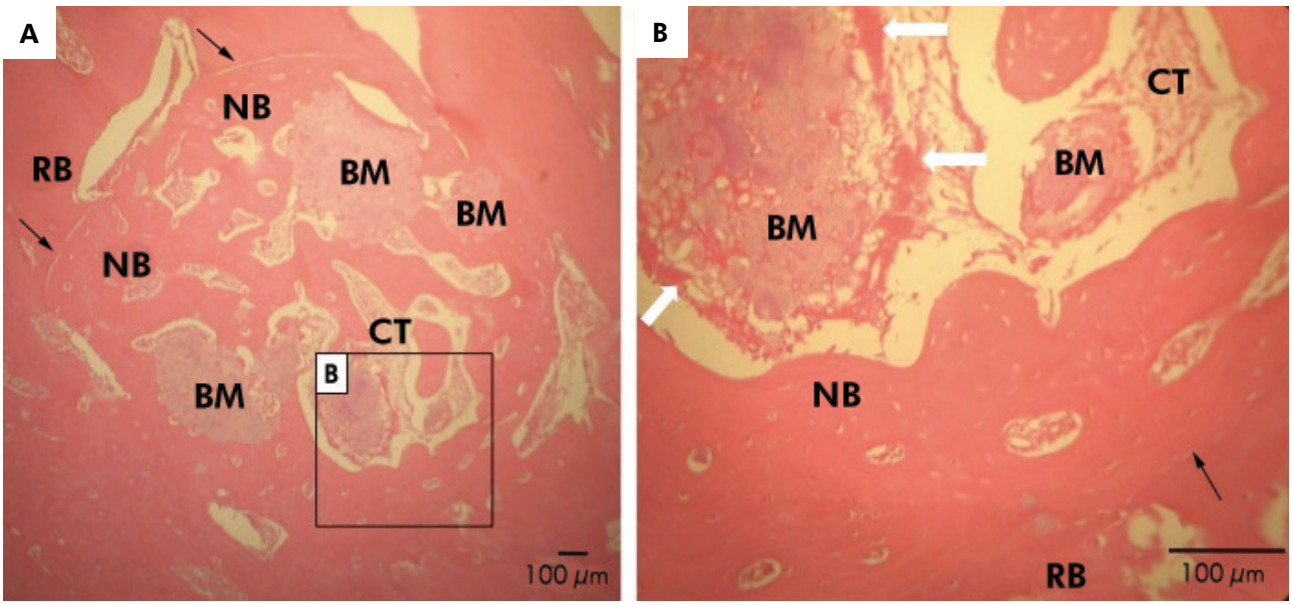

Figure 4. Representative photomicrographs of the HA group. Defect area (black arrow); newly formed bone (NB); central area of the defect composed of loose connective tissue (CT) with sparse chronic inflammatory infiltrate and few multinucleated giant cells (white arrows) surrounding the biomaterial particles (BM).

of phosphorus and calcium. In the HA and SrHA groups, three points were scored: biomaterial, newly formed bone and preexisting bone. In both of these groups, large quantities of calcium and phosphorus were observed. In the SrHA group, no strontium was detected in the sample (data not shown).

X-ray microfluorescence with synchrotron radiation

The results of microfluorescence with X-ray synchrotron radiation (µXRF-SR) of the sample shafts revealed the presence of common elements of mature bone, including calcium, strontium, potassium and zinc (Figure 7). In the micrographs corresponding to calcium, potassium and zinc, larger amounts of ions were evident in the cortical bone, in contrast with strontium, which was abundant in the region of biomaterial placement. In addition, a yellow halo was observed surrounding the SrHA material, suggesting the existence of an interaction between the strontium of the biomaterial and the biological medium.

Histomorphometric Evaluation

Quantitative descriptions of the newly formed bone, biomaterial and connective tissue densities are provided in Figure 8A, 8B and 8C, respectively. Histomorphometric analysis confirmed the histological findings. The control (36.4 ± 21.8), HA (31.2 ± 14.7) and SrHA (26.2 ± 12.1) groups did not exhibit significant differences in newly formed bone density ($p > 0.05$). Volume density analyses of the biomaterials revealed the presence of significant differences among the groups, with the SrHA group showing a higher volume density of biomaterial (51.2 ± 14.1) compared to the HA group (36.2 ± 8.5) ($p = 0.03$). Analyses of the volume densities of connective tissue indicated that there were no significant differences among the clot (36.4 ± 21.8), HA (36.2 ± 20.1) and SrHA (22.6 ± 15.5) groups ($p > 0.05$).

Discussion

In the present study, small defects were created in sheep tibia, with the aim of evaluating the biocompatibility and bone healing after implantation of microspheres of hydroxyapatite (HA) and 1% strontium-containing nanostructured hydroxyapatite (SrHA). Thus, a defect of 2 mm in diameter was sufficient and associated with a minimal risk of bone fracture.

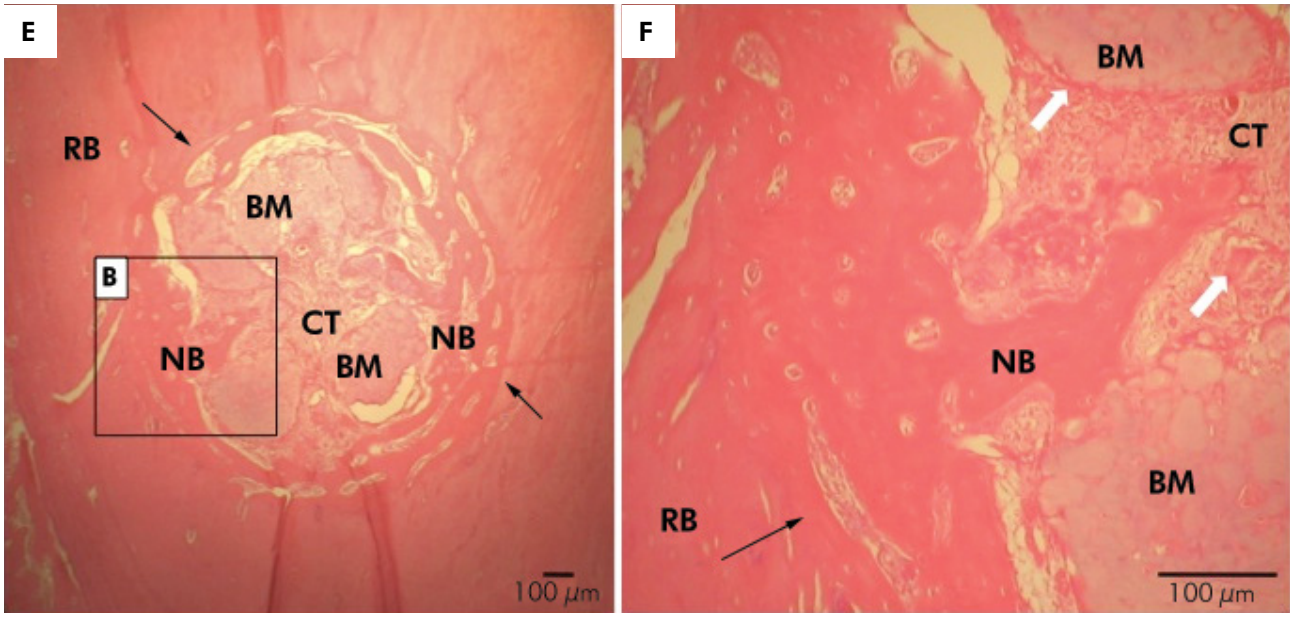

Figure 5. Representative photomicrographs of the SrHA group. Defect area (black arrow); newly formed bone (NB); central area of the defect composed of loose connective tissue (CT) with sparse chronic inflammatory infiltrate and multinucleated giant cells (white arrows) surrounding the biomaterial particles (BM).

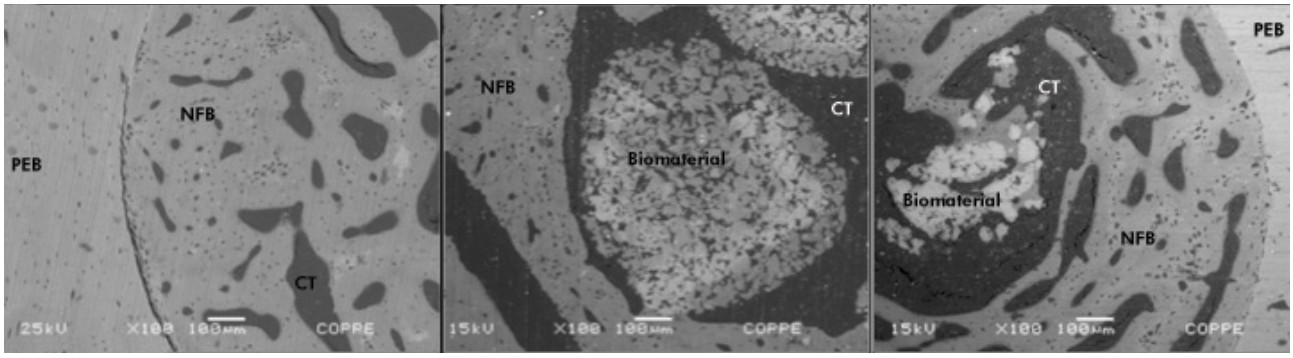

Figure 6. Scanning electron microscopy (SEM) micrographs. (A) Control group; (B) HA group; (C) SrHA group. NFB: newly formed bone; PEB: pre-existing bone; and CT: connective tissue; magnification: 100X.

The use of sheep in research has increased over time because of their similarities with humans in weight, bone structure and joint and bone regeneration.[21,22] A previous study has shown the effectiveness of drilling in a sheep model used to evaluate the biocompatibility of biomaterial bone substitutes, demonstrating the possibility of implanting up to 8 types of biomaterials per animal.[23,24] Another important benefit of this model is that it allows for the maintenance of the living animal after the experiment, which is consistent with the worldwide principles of the 3Rs (Refinement, Reduction and Replacement).

According to the histological findings, the defects that were not filled with biomaterial and were filled only with blood clots, newly formed bone was observed. These results are consistent with those of previous studies on the repair of critical- and non-critical-sized defects, with bone formation from the periphery to the center of the defect.[4,13] Moreover, evaluation of the tissue responses to different biomaterials implanted in sheep tibias showed that they exhibited granulation reactions to the biomaterials that were confined to the implant sites, characterized by chronic inflammation. It is well known that anorganic xenografts and

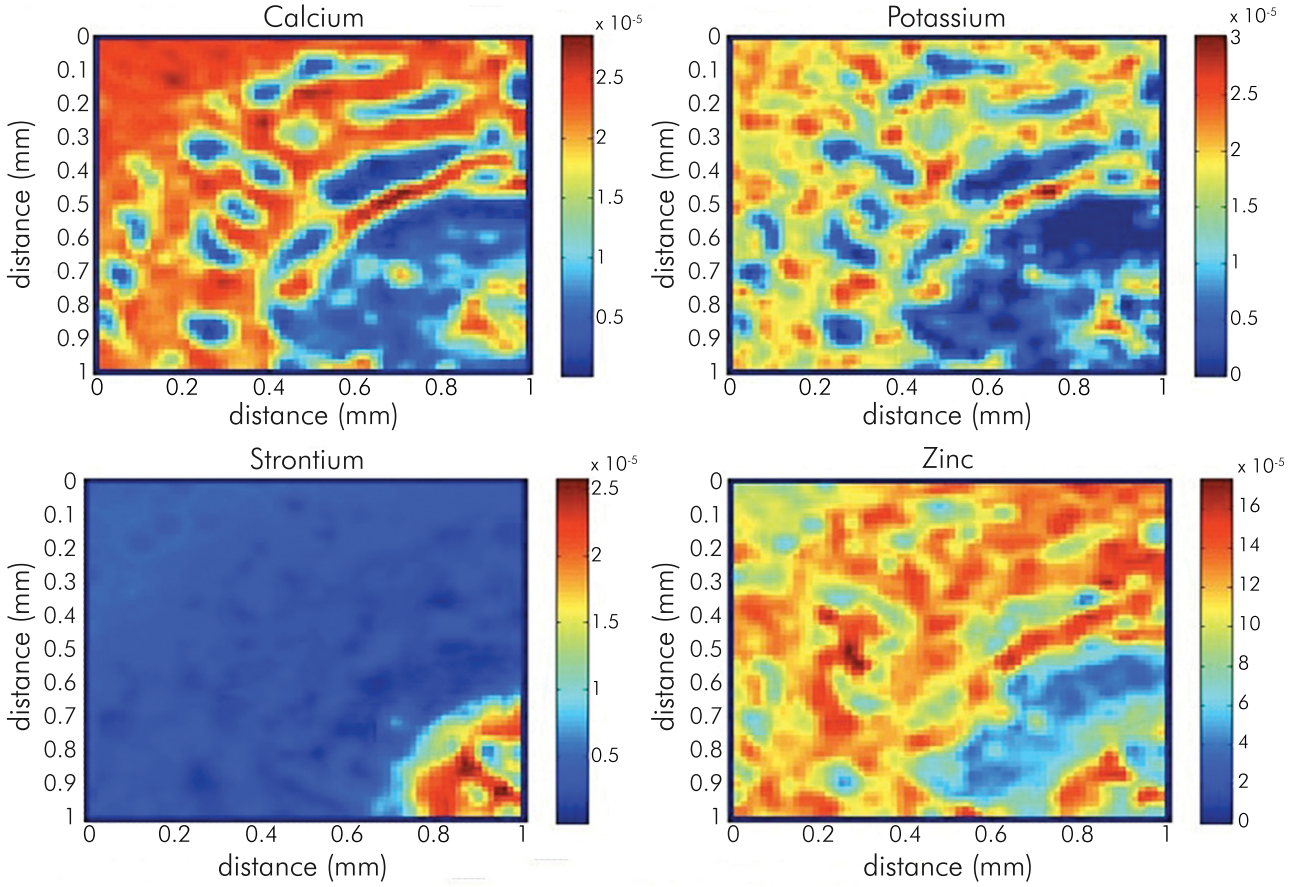

Figure 7. μXRF-SR spatial distribution of strontium from SrHA microspheres after 30 days post-implantation.

synthetic hydroxyapatite implants result in a foreign body-like granulomatous reactions.[25,26] It must be emphasized however, that the presence of giant cells occurs in an attempt of the organism to reabsorb the material and does not necessarily imply a lack of biocompatibility.

Synthetic HA differs from biological apatite in a number of important ways. Several studies have attempted to mitigate these differences by doping synthetic HA with small amounts of impurities, thereby altering its properties, including its crystallinity, morphology, lattice parameters, stability, solubility and mechanical characteristics.[27,28] Many studies have attempted to change the composition of HA to better understand and improve the tissue response after HA implantation. The inorganic component of bone tissue is a nonstoichiometric carbonated apatite containing substitutions of Na^+, K^+, Mg^{2+}, Sr^{2+}, Cl^-, F^-, HPO_4 or Zn^{2+}.[27] The presence of trace elements may affect bone formation and resorption through direct or indirect effects on bone cells or bone minerals.[29] Rapid release of calcium and strontium ions from soluble strontium-doped hydroxyapatite can also lead to issues with cytotoxicity.[30,31] Therefore, it is necessary to strike a balance between solubility and cytotoxicity, such that the amount of strontium-containing HA incorporated is sufficient to improve solubility without inducing significant cytotoxicity.

Our study showed that 1% strontium-containing nanostructured hydroxyapatite is biocompatible, exhibiting close contact with newly formed bone with no significant differences when compared with the HA group. These results contradict the findings of Dagang et al.,[32] who evaluated a strontium-containing HA cement and showed that it had better osteoconductivity, biocompatibility and biodegradability than HA-only cement. Biocompatibility testing performed by these authors revealed that the 5% strontium-containing

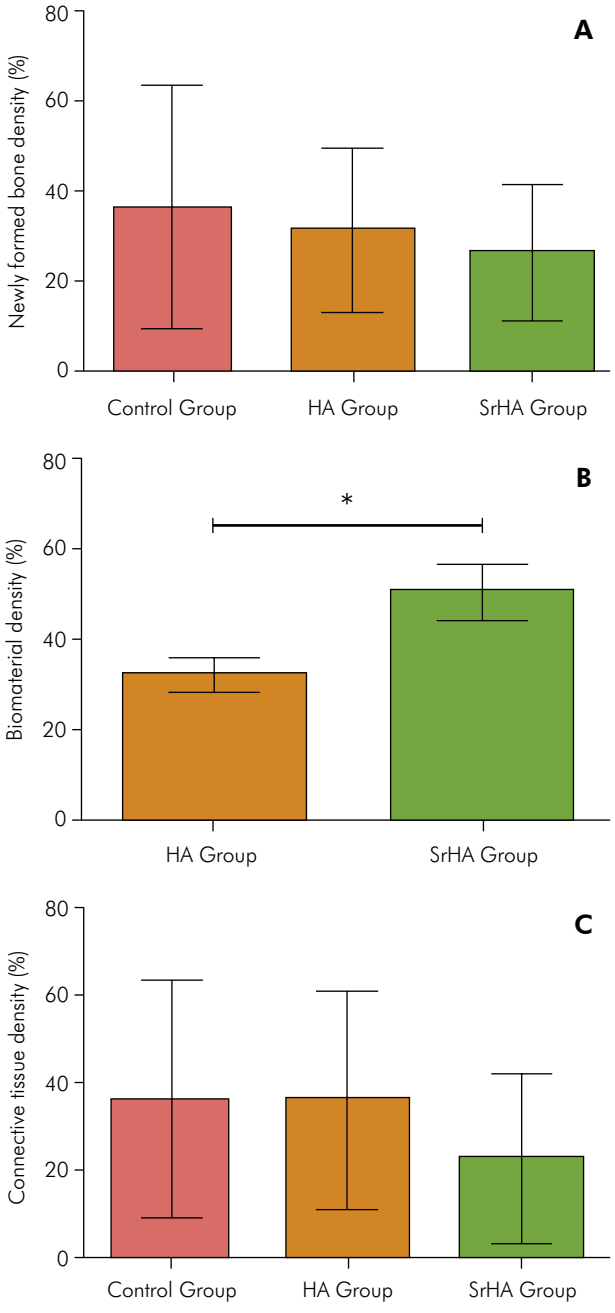

Figure 8. Newly formed bone densities (A), biomaterial densities (B) and connective tissue densities (C) of the control, HA and SrHA groups at 30 days post-implantation. (*) represents a significant difference among the groups at same experimental time point (Wilcoxon signed-rank test, $p \leq 0.05$). The results are shown as the mean percentage ± confidence interval.

HA cement was the most biocompatible, followed by 10% strontium-containing HA cement and finally, HA-only cement without strontium. These data indicate that there is an optimal dose of strontium for incorporation into crystal HA to achieve the best physicochemical properties and biocompatibility.[33]

Wong et al.[20] performed an *in vivo* study investigating the responses of injection of Sr-containing HA bone cement into cancellous bone from the iliac crests of rabbits after 1, 3 and 6 months. The bone affinity to the Sr-containing HA cement increased from 73.55% ± 3.50% after 3 months to 85.15% ± 2.74% after 6 months ($p = 0.01$). These results demonstrated that Sr-containing HA cement is biocompatible and osteoconductive, supporting the data obtained in the present study, despite the fact that our trial period was only 30 days. Valiense et al.[13] evaluated 5% strontium-containing nanostructured carbonated HA/sodium alginate microspheres placed into rabbit sinuses and showed that this biomaterial was biocompatible and osteoconductive, also supporting the data obtained in this study.

The X-ray microfluorescence with synchrotron radiation results confirmed the presence of the strontium ion in the SrHA biomaterial group. A yellow halo was also observed around the SrHA spheres, suggesting that strontium was released into the bone around the defect (Figure 5).

A previous *in vitro* study evaluated the bioactivity of strontium-containing HA in simulated body fluid, along with its effects on proliferation and cell morphology. The strontium-containing hydroxyapatite ceramic exhibited high bioactivity in simulated body fluid, as evidenced by the rapid formation of apatite on its surface. The cell culture test indicated that the Sr-containing HA ceramic had good biocompatibility with human osteoblasts. Compared with HA, the Sr-containing HA ceramic did not have any deleterious effects on extracellular matrix formation or mineralization.[34] In another study,[35], osteoblast cells cultured in strontium-containing hydroxyapatite had normal morphologies, good proliferative capacities and increased values for several differentiation parameters; however, the number of osteoclasts was negatively influenced by the presence of Sr. The positive effect of this ion on bone cells was particularly evident in the case of deposition of Sr-containing HA at relatively high doses (3-7%), with significant increases in alkaline phosphatase activity and osteocalcin, type I collagen and osteoprotegerin/TNF levels in association with cytokine receptors.

In summary, the present study has demonstrated that spheres of 1% strontium-containing nanostructured hydroxyapatite have biocompatible and osteoconductive properties similar to stoichiometric hydroxyapatite in bone repair. However, additional future studies must be performed to obtain a detailed understanding of the cellular and molecular mechanisms of the effects of strontium on bone cells and the optimal strontium concentration.

Conclusions

Microspheres of nanostructured HA and SrHA (1%) exhibit biocompatible and osteoconductive properties and may be indicated as bone substitutes for clinical applications. Future studies assessing the use of different concentrations are needed to optimize the biological response.

Acknowledgments

The authors acknowledge *Laboratório Nacional de Luz Síncrotron* – LNLS, *Instituto Alberto Luiz Coimbra de Pós-Graduação e Pesquisa de Engenharia / Universidade Federal do Rio de Janeiro* – COPPE/UFRJ and *Fundação de Amparo à Pesquisa do Estado do Rio de Janeiro* – FAPERJ for their financial support, which enabled this study to be performed.

References

1. Lekovic V, Kenney EB, Weinlaender M, Han T, Klokkevold PR. A bone regenerative approach to alveolar ridge maintenance following tooth extraction. Report of 10 cases. J Periodontol. 1997;68(6):563-70. doi:10.1902/jop.1997.68.6.563
2. Melloning JT, Triplett RG. Guided tissue regeneration and endosseous dental implants. Int J Periodontics Restorative Dent. 1993;13(2):109-19.
3. Hallman M, Mordenfeld A, Strandkvist T. Bone replacement following dental trauma prior to implant surgery: status. Dent Traumatol. 2009;25(1):2-11. doi:10.1111/j.1600-9657.2008.00690.x.
4. Calasans-Maia M, Calasans-Maia J, Santos S, Mavropoulos E, Farina M, Lima I, et al. Short-term in vivo evaluation of zinc-containing calcium phosphate using a normalized procedures. Mater Sci Eng C Mater Biol Appl. 2014 Aug 1;41:309-19. doi:10.1016/j.msec.2014.04.054.
5. Oikarinen KS, Sàndor GKB, Kainulainen VT, Salonen-Kemppi M. Augmentation of the narrow traumatized anterior alveolar ridge to facilitate dental implant placement. Dent Traumatol. 2003;19(1):19-29. doi:10.1034/j.1600-9657.2003.00125.x
6. Klijn RJ, Meijer GJ, Bronkhorst EM, Jansen JA. A meta-analysis of histomorphometric results and graft healing time of various biomaterials compared to autologous bone used as sinus floor augmentation material in humans. Tissue Eng Part B Rev. 2010;16(5):493-507. doi:10.1089/ten.teb.2010.0035
7. Boyne PJ, Sands NR. Combined orthodontic-surgical management of residual palato-alveolar cleft defects. Am J Orthod. 1976;70(1):20-37. doi:10.1016/0002-9416(76)90258-X
8. Dahlin C, Andersson L, Linde A. Bone augmentation at fenestrated implants by an osteopromotive membrane technique. A controlled clinical study. Clin Oral Implants Res. 1991;2(4):159-65. doi:10.1034/j.1600-0501.1991.020401.x
9. Suchanek W, Yoshimura M. Processing and properties of hydroxyapatite-based biomaterials for use as hard tissue replacement implants. J Mater Res. 1998;13(1):94-117. doi:10.1557/JMR.1998.0015
10. Aina V, Bergandi L, Lusvardi G, Malavasi G, Imrie FE, Gibson IR, et al. Sr-containing hydroxyapatite: morphologies of HA crystals and bioactivity on osteoblast cells. Mater Sci Eng C. 2013;33(3):1132-42. doi:10.1016/j.msec.2012.12.005
11. Yan J, Sun JF, Chu PK, Han Y, Zhang YM. Bone integration capability of a series of strontium-containing hydroxyapatite coatings formed by micro-arc oxidation. J Biomed Mater Res A. 2013;101(9):2465-80. doi:10.1002/jbm.a.34548
12. Ammann P, Shen V, Robin B, Mauras Y, Bonjour JP, Rizzoli R. Strontium ranelate improves bone resistance by increasing bone mass and improving architecture in intact female rats. J Bone Miner Res. 2004;19(12):2012-20. doi:10.1359/jbmr.040906
13. Valiense H, Barreto M, Resende RF, Alves AT, Rossi AM, Mavropoulos E, et al. In vitro and in vivo evaluation of strontium-containing nanostructured carbonated hydroxyapatite/sodium alginate for sinus lift in rabbits. J Biomed Mater Res B Appl Biomater. 2016 Feb;104(2):274-82. doi:10.1002/jbm.b.33392. Epub 2015 Feb 26.
14. Marie PJ, Ammann P, Boivin G, Rey C. Mechanisms of action and therapeutic potential of strontium in bone. Calcif Tissue Int. 2001;69(3):121-9. doi:10.1007/s002230010055
15. Canalis E, Hott M, Deloffre P, Tsouderos Y, Marie PJ. The divalent strontium salt S12911 enhances bone cell replication and bone formation in vitro. Bone. 1996;18(6):517-23. doi:10.1016/8756-3282(96)00080-4
16. Lindahl C, Engqvist H, Xia W. Effect of strontium ions on the early formation of biomimetic apatite on single crystalline rutile. Appl Surf Sci. 2013;266(1):199-204. doi:10.1016/j.apsusc.2012.11.147

17. Xu JL, Khor KA, Sui JJ, Zhang JH, Chen WN. Protein expression profiles in osteoblasts in response to differentially shaped hydroxyapatite nanoparticles. Biomaterials. 2009;30(29):5385-91. doi:10.1016/j.biomaterials.2009.07.002
18. Hulsart Billström G, Xia W, Pankotai E, Weszl M, Carlsson E, Engqvist H, et al. Bone forming potential of Sr doped hydroxyapatite hollow spheres in a rat vertebral bone defect model. Bone. 2012;50(Suppl 1):S114. doi:10.1016/j.bone.2012.02.352
19. Shen Y, Liu J, Lin K, Zhang W. Synthesis of strontium substituted hydroxyapatite whiskers used as bioactive and mechanical reinforcement material. Mater Lett. 2012;70(1):76-9. doi:10.1016/j.matlet.2011.11.093
20. Wong CT, Chen QZ, Lu WW, Leong JC, Chan WK, Cheung KMC, et al. Ultrastructural study of mineralization of a strontium-containing hydroxyapatite (Sr-HA) cement in vivo. J Biomed Mater Res A. 2004;70(3):428-35. doi:10.1002/jbm.a.30097
21. Augat P, Margevicius K, Simon J, Wolf S, Suger G, Claes L. Local tissue properties in bone healing: influence of size and stability of the osteotomy gap. J Orthop Res. 1998;16(4):475-81. doi:10.1002/jor.1100160413
22. Nunamaker DM. Experimental models of fracture repair. Clin Orthop Relat Res. 1998;355 Suppl:S56-65. doi:10.1097/00003086-199810001-00007
23. Habibovic P, Gbureck U, Doillon CJ, Bassett DC, van Blitterswijk CA, Barralet JE. Osteoconduction and osteoinduction of low-temperature 3D printed bioceramic implants. Biomaterials. 2008;29(7):944-53. doi:10.1016/j.biomaterials.2007.10.023
24. Nuss KMR, Auer JA, Boss A, von Rechenberg B. An animal model in sheep for biocompatibility testing of biomaterials in cancellous bones. BMC Musculoskelet Disord. 2006;7:67. doi:10.1186/1471-2474-7-67
25. Oliveira RC, Sicca CM, Silva TL, Cestari TM, Oliveira DT, Buzalaf MAR, et al. [Effect of deproteinization temperature on the preparation of microgranular bovine cortical bone. Microscopic and biochemical analysis in rat subcutaneous tissue]. Rev Faculdade Odontol Bauru. 1999;7(3-4):85-93. Portuguese.
26. Zambuzzi WF, Oliveira RC, Pereira FL, Cestari TM, Taga R, Granjeiro JM. Rat subcutaneous tissue response to macrogranular porous anorganic bovine bone graft. Braz Dent J. 2006;17(4):274-8. doi:10.1590/S0103-64402006000400002
27. Bigi A, Boanini E, Bracci B, Facchini A, Panzavolta S, Segatti F, et al. Nanocrystalline hydroxyapatite coatings on titanium: a new fast biomimetic method. Biomaterial. 2005;26(19):4085-9. doi:10.1016/j.biomaterials.2004.10.034
28. Webster TJ, Massa-Schlueter EA, Smith JL, Slamovich EB. Osteoblast response to hydroxyapatite doped with divalent and trivalent cations. Biomaterials. 2004;25(11):2111-21. doi:10.1016/j.biomaterials.2003.09.001
29. Landi E, Logroscino G, Proietti L, Tampieri A, Sandri M, Sprio S. Biomimetic Mg-substituted hydroxyapatite: from synthesis to in vivo behaviour. J Mater Sci Mater Med. 2008;19(1):239-47. doi:10.1007/s10856-006-0032-y
30. Bauer IW, Li SP, Han YC, Yuan L, Yin MZ. Internalization of hydroxyapatite nanoparticles in liver cancer cells. J Mater Sci Mater Med. 2008;19(3):1091-5. doi:10.1007/s10856-007-3124-4
31. Watari F, Yokoyama A, Gelinsky M, Pompe W. Conversion of functions by nanosizing from osteoconductivity to bone substitutional properties in apatite. In: Watanabe M, Okuno O, Sasaki K, Takahashi N, Suzuki O, Takada H, editors. Interface Oral Health Science 2007. Proceedings of the 2nd International Symposium for Interface Oral Health Science; 18-19 Sept 2007; Sendai, Japan. New York: Springer; 2007. p. 139-47. doi:10.1007/978-4-431-76690-2_13
32. Dagang G, Kewei X, Yong H. The influence of Sr doses on the in vitro biocompatibility and in vivo degradability of single-phase Sr-incorporated HAP cement. J Biomed Mater Res A. 2008;86(4):947-58. doi:10.1002/jbm.a.31687
33. Christoffersen J, Christoffersen MR, Kolthoff N, Bärenholdt O. Effects of strontium ions on growth and dissolution of hydroxyapatite and on bone mineral detection. Bone. 1997;20(1):47-54. doi:10.1016/S8756-3282(96)00316-X
34. Xue W, Moore JL, Hosick HL, Bose S, Bandyopadhyay A, Lu WW, et al. Osteoprecursor cell response to strontium-containing hydroxyapatite ceramics. J Biomed Mater Res A. 2006;79(4):804-14. doi:10.1002/jbm.a.30815
35. Capuccini C, Torricelli P, Sima F, Boanini E, Ristoscu C, Bracci B, et al. Strontium-substituted hydroxyapatite coatings synthesized by pulsed-laser deposition: in vitro osteoblast and osteoclast response. Acta Biomater. 2008;4(6);1885-93. doi:10.1016/j.actbio.2008.05.005